ACS Photonics

ACS EDITORS' CHOICE

pubs.acs.org/journal/apchd5

Article

Flash Brillouin Scattering: A Confocal Technique for Measuring Glass Transitions at High Scan Rates

Konrad Rolle,* Hans-Jürgen Butt, and George Fytas

Cite This: *ACS Photonics* 2021, 8, 531−539

Read Online

ACCESS | Metrics & More | Article Recommendations

ABSTRACT: Glass transition temperatures T_g are most commonly measured by differential scanning calorimetry, a method that has been extended to the flash scanning calorimetry (FSC) regime by reducing sample volumes. However, significant manual preparation effort can render FSC impractical for, e.g., local probing of spatially heterogeneous specimens. Another strategy can be to select a small volume by focusing down a laser beam, where Brillouin Light Scattering (BLS) is a proven method for confocal T_g measurement. Here, we introduce Flash Brillouin Scattering, which extends BLS to fast scan rates, achieved by periodically heating the probed region with an infrared laser. For comparison with conventional BLS, we first characterize T_g of pure glycerol, and show how rapid quenching produces a less packed glass with downshifted sound velocity. We then turn toward its aqueous solutions, which crystallize too fast for a nonflash approach, and demonstrate scan rates in excess of 10^5 K/s. These results are of interest not only because glycerol is a model system for hydrogen-bonded glass formers, but also because of its applications as a cryoprotectant for frozen biological samples. Light scattering studies of the latter, currently limited to cryo-Raman spectroscopy, are likely to be complemented by the technique introduced here.

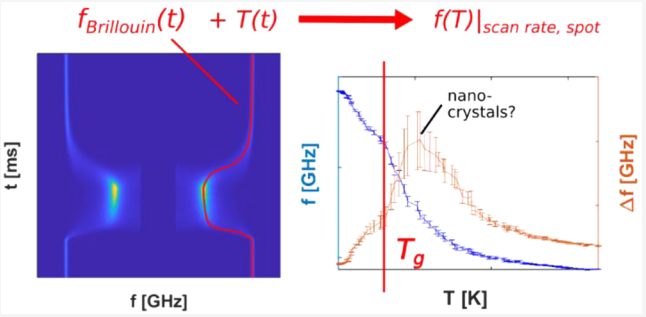

KEYWORDS: *Brillouin light scattering, glass transition, crystallization, time-resolved, thermometry, cryoprotectant*

Several techniques exist for characterizing the glass transition temperature T_g, most of which, however, are limited to quasi-static scan (heating and cooling) rates. This not only belies the dynamic identity of any assigned T_g value, but becomes a definite obstacle once systems with high crystallization rates are to be investigated. Thus, differential scanning calorimetry (DSC), the most widely available T_g analysis method, has to be extensively modified for so-called "Flash Scanning Calorimetry" (FSC)[1] experiments: Due to finite thermal diffusion, small (typically, nanogram) sample volumes are required to achieve rapid quenching and flash heating of, e.g., semicrystalline polymers. This not only increases constraints on the sensor, manufactured with MEMS technology from fragile single-use silicon nitride membranes. It also has to be accompanied by a significant manual preparation effort, which involves cutting the specimen down to μm-dimensions and positioning it on the ∼100 nm thin substrate. As a result, if the measurement has to be repeated many times due to, for example, large statistical variations, or nondestructive in situ probing is the objective, an alternative to FSC is needed.

Optical T_g measurement, by virtue of its noncontact character, was quick to achieve results on samples with extreme dimensions long before nanocalorimetry gained prominence. Ellipsometry is widely available and convenient for examining T_g in the specific case of ultrathin films on a glass substrate,[2,3] where T_g is deduced from a temperature-dependent change in differential film thickness. For more general cases, however, frequency-domain Brillouin Light Scattering (BLS)[4] is preferred, which is not limited to thin films or other sample geometries. While the context of these early studies were confinement effects on length scales less than 100 nm, we will aim to show here how the same technology can be repurposed for "flash" experiments for which FSC is ill-adapted. Indeed, by focusing down a laser beam with an appropriate objective lens, μm-sized volumes can easily be selected in BLS, akin to other confocal microscopy techniques. Though confocal Brillouin spectroscopy has seen a surge of interest over the past decade for mechanical bioimaging,[5,6] its potential utility for flash T_g determination has seemingly not been noticed yet. Compared with FSC, a confocal technique would be particularly advantageous for

Received: October 2, 2020
Published: December 28, 2020

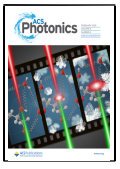

https://dx.doi.org/10.1021/acsphotonics.0c01533
ACS Photonics 2021, 8, 531−539

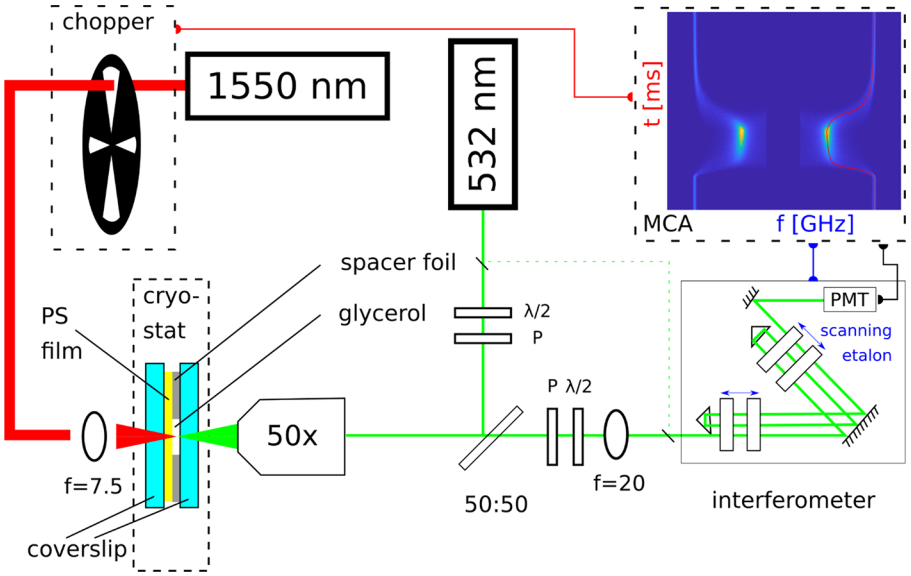

Figure 1. Flash Brillouin Scattering (FBS) setup with pure glycerol sample configuration in cryostat, comprising a polystyrene (PS) thin film. The thin green line represents the beam path of the visible ("532 nm") probe-laser in backscattering configuration, showing microscope objective ("50×", f = 4 mm), polarizers ("P"), half-waveplate ("$\lambda/2$"), beamsplitter (50:50), and a lens (f = 200 mm) with focal point on the spectrometer entrance pinhole. The thick red line represents the beam path for the amplified infrared ("1550 nm") heating laser, with chopper and focusing asphere (f = 7.5 mm). A multichannel analyzer (MCA) registers chopper and scanning etalon (mirror) positions on each count from the photomultiplier tube (PMT), which are then processed into a bidimensional histogram (inset MCA-frame plot, showing central portion of 50 wt % case 2D-histogram for T_i = 123 K, with a thin red line marking Lorentzian peak position).

local probing or imaging of a structure with spatially heterogeneous T_g distribution, since several points on the same sample can easily be checked this way.

A spatial T_g map can be constructed using atomic force microscopy (AFM), an approach that often goes by the name of local thermal analysis (LTA),[7,8] boasts resolution below 100 nm[9,10] and is commercially available.[11] Setting aside the question of how such a quasi-static T_g probe translates to high scan rates,[12] AFM is limited to probing the sample surface, with which contact has to be established. Hence, rather than polymers, we will concentrate on molecular liquids, using glycerol as a model glass former. Indeed, confocal microscopy is much better adapted for studying liquids than AFM, since the liquid can be enclosed in a transparent cell, while the exposed liquid/gas interface probed by AFM is susceptible to evaporation[13] (a drawback also of the open-air[14] FSC sensor). Furthermore, glycerol has widely featured not only in fundamental T_g studies, but is also of practical interest for applications as a cryoprotectant when freezing, e.g., embryos[15,16] or other biological material for preservation at liquid-nitrogen temperatures. Finally, by choosing glycerol, we can first validate our technique by comparing results with existing BLS data,[17] as measured by quasi-static methods. By adding water, we then produce an aqueous solution which, for compositions of typically less than 75 wt % glycerol (termed the "maximally freeze concentrated solution" or MFCS[18]) will crystallize if the quench is not sufficiently rapid. Hence, the mixed system cannot be examined by conventional BLS and requires a new method of T_g determination, to be introduced in this paper and referred to as "Flash Brillouin Scattering" (FBS) by analogy with FSC in what follows.

BLS is an inelastic light scattering technique similar to Raman spectroscopy insofar as an incident laser beam interacts with vibrations ("phonons"). Resolving scattered light in a spectrometer then allows for deduction of vibration frequency and, hence, material properties. However, while Raman looks at individual molecular vibrations, BLS is sensitive to lower frequency GHz acoustic phonons ("sound waves") from the collective motion of the solid, whence its main use for elasticity measurement. However, this also renders it superior to Raman[19−21] at detecting cooperative phenomena like the glass transition. Accordingly, it has been widely used for this purpose[22,23] as well as the related one of deducing GHz structural relaxation times from temperature scans for the frequency at which the hypersonic loss maximum (phonon lifetime minimum) occurs.[24] While for bioimaging applications a dispersive spectrometer design based on a prism called "virtually imaged phased array" (VIPA) is adopted,[25,5] only tentative steps[26] have been undertaken to exploit VIPA for T_g studies, which remain dominated by instruments based on scanning Fabry−Perot etalons. The latter, while significantly slower than VIPA because detectors are not multichannel, offer optimum frequency-resolution and contrast ratio, as well as proven[27] time-resolved measurement capabilities; both instrument variants can be easily[28,29] made to share the beam path with a Raman spectrometer. In the particular context of low-temperature biology, Raman has already established itself[30] as a tool for mapping cryoprotectant and ice distribution[31,32] and even for studying phase transitions.[33] Due to their technical similarity, we expect FBS to eventually come to extend the cryo-Raman toolbox, particularly if complementary low-temperature biology uses for BLS (e.g., strain sensing[34−36]) can be found.

EXPERIMENTAL SECTION

The BLS setup is based on a tandem-triple-pass Fabry−Perot (TFP) interferometer (JRS TFP-2HC) equipped with a narrow-linewidth laser (532 nm, 300 mW, Spectra-Physics Excelsior). Separation of the mirror pairs (etalons) inside the TFP is piezoelectrically scanned to analyze scattered light

https://dx.doi.org/10.1021/acsphotonics.0c01533
ACS Photonics 2021, 8, 531−539

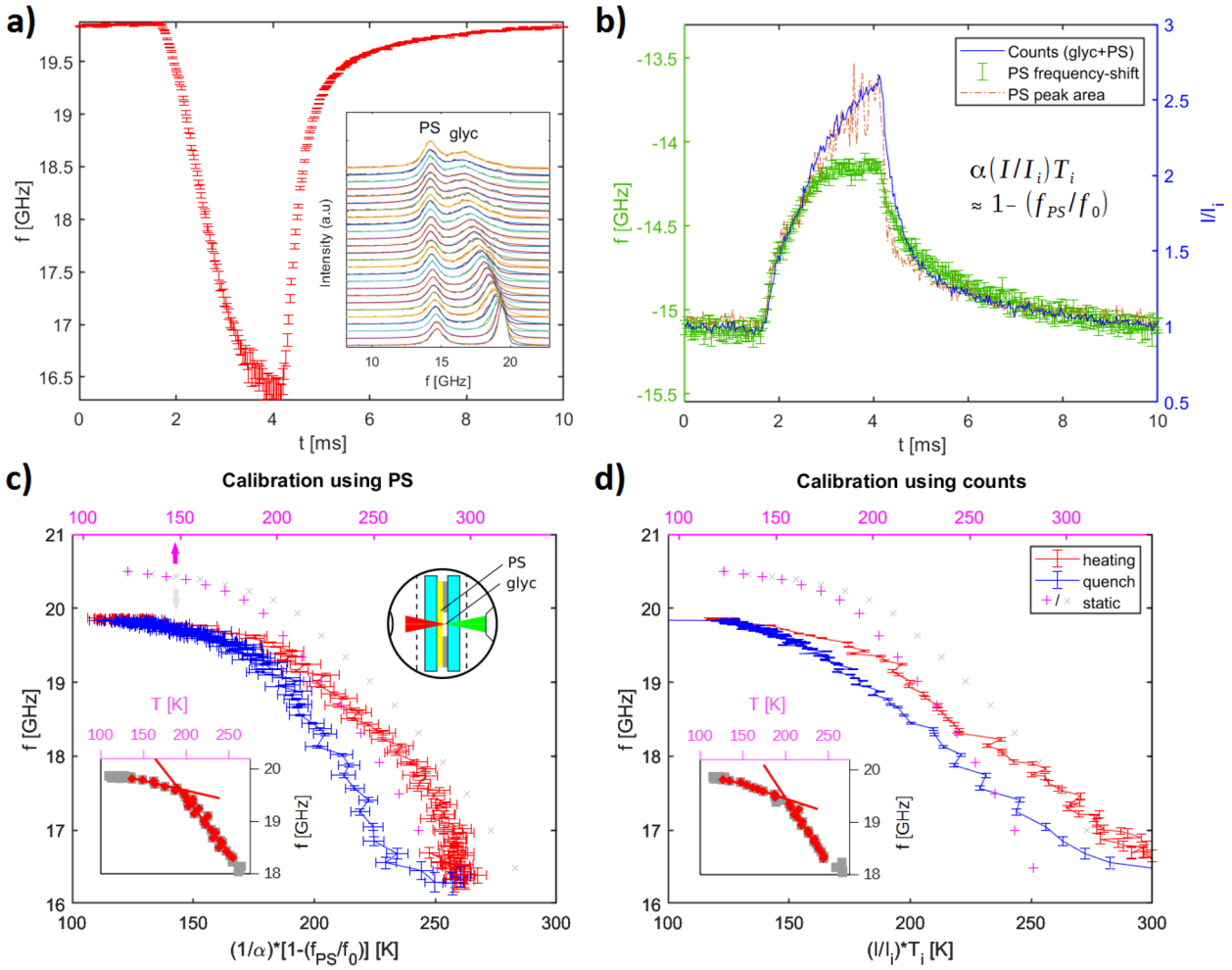

Figure 2. FBS data for pure glycerol: (a) time-evolution of the glycerol frequency-shift in backscattering geometry, obtained from the Lorentzian representation of the BLS spectra; the inset shows selected spectra, sampled on the heating cycle (differential time interval for sampling $\Delta t \sim 0.07$ ms) and displaying two phonon peaks assigned to polystyrene (PS, low frequency) and glycerol (high frequency); (b) time-evolution of PS peak area $\sim I_{PS}(t)/I_{PS}(t_0)$ and the two variables used for temperature calibration, PS frequency-shift $f_{PS}(t)$ (note negative frequencies) and integrated detector counts $I(t)/I(t_0)$, the latter due to both PS and glycerol inelastic scattering; identifying left- and right-hand y-axes, the differential frequency shift α for $f_{PS}(T)$ is deduced; (c) glycerol temperature calibrated using the frequency-shift $f_{PS}(T)$ from the PS thin film (see top right inset), with heating and cooling cycles distinguished by color for convenience; at high temperature, agreement of the heating cycle with reference data from quasi-static BLS (tilted crosses) is improved (upright crosses) by a linear transformation of the x-axis at fixed T_i, so that the glass point can be found from the intersection of the linear fits for regions above and below T_g (bottom left inset); (d) similar to (c), but with glycerol temperature calibrated using time-evolution of integrated detector counts $I(t)/I(t_0)$; legend applies to both (c) and (d).

within a configurable frequency interval (free spectra range, FSR). In order to add time-resolved measurement capabilities, the manufacturer-provided one-dimensional multichannel analyzer (MCA) for spectrally resolving scattered light as a function of the scanning etalon position is replaced with a time-stamped MCA. The latter is custom-built from a programmable timer-counter board (NI PCIe-6612), similar to what can be found in photon correlation spectroscopy (PCS).[37] Two counters are set up for the scanning etalon and an external asynchronous reference signal, where the latter is incremented every 50 ns. The current counter tallies are saved each time the TFP photomultiplier tube (Hamamatsu H10682, 1.3 ns jitter, quantum efficiency 14%) registers a pulse, and each counter is reset by its respective control signal. MCA input is blocked by an RF-switch (Mini-Circuits ZYSWA-2−50DR+) during the central scan portion, when a shutter unit (JRS LM-2) rejects elastically (Rayleigh) scattered sample light. The obtained 2D-array can then be processed into a bidimensional histogram by MATLAB (see inset of MCA-frame in Figure 1) with adjustable bin numbers (typical time-bin number up to 500), and Lorentzian fits (peak position given by red line in histogram plot) performed for the spectra corresponding to each time instant.

For FBS, the external reference signal follows a periodic temperature cycle induced by heating pulses in the sample. In order to preserve the BLS advantages of noncontact, nondestructive, and high spatial resolution measurement, sample heating is accomplished by a second laser at 1550 nm, amplified to 1−2 W by an erbium-doped fiber amplifier (EDFA, civillaser.com). Heating pulses and their corresponding reference signal are then generated by a chopper (Thorlabs MC2000B) with an adjustable duty cycle blade (MC1F10A) set at 25%. This duty cycle is low enough to provide the system time to relax to its initial temperature, T_i. The latter is imposed by means of a Linkam (HFS 350EV-PB4) liquid nitrogen stage vertically mounted by a custom holder in the spectrometer,

https://dx.doi.org/10.1021/acsphotonics.0c01533
ACS Photonics 2021, 8, 531−539

while the sample is pressed against the stage body by the spring-force of an L-shaped handle with magnetic base. Thermal contact is assured by a Panasonic pyrolitic graphite sheet, and air/nitrogen are blown across both front and back windows to prevent condensation.

Two systems are investigated, pure glycerol and an aqueous mixture (50 wt %). For both, the sample consists in a drop of liquid sandwiched between two coverslips, separated by 2 μm ultrathin aluminum spacer foil (Alfa Aesar). For the aqueous mixture, the 1550 nm laser can heat the system under study directly, due to the proximity of its wavelength to the 1480 nm water absorption peak. For pure glycerol, absorption is low, so an additional ∼2 μm polystyrene (molecular weight MW = 200 kDa) thin film is spin-cast[38,39] from toluene solution to which a broadband infrared dye (Epolight 1125) has been added at less than 1 wt %. Also, for confining pure glycerol in the sample cell, the coverslips are preheated, which reduces glycerol viscosity and makes it easier to achieve the target thickness.[40] For both systems, overnight vacuum drying at 100 °C is used to remove any excess water prior to sample assembly; for the mixture, Milli-Q water is then readded to achieve the desired concentration. Finally, the stage is flooded with nitrogen atmosphere and the samples are cooled down to T_i = 123 K at the maximum rate of 30 K/min permitted by the cryostat. For the aqueous mixture, T_i = 88 K was also examined.

Back scattering geometry, where incident and scattered light pass through a single objective (Nikon CFI T Plan Epi SLWD 50×), is used for the probe laser, polarizer orientations (see Figure 1) being the same in both paths. The Linkam stage is orientated at 15° to avoid sending the reflection from the sample toward the spectrometer entrance; this reduces laser noise and thereby obviates the need for a cleanup filter (e.g., JRS TCF-1). FSRs were set to 25 and 40 GHz for pure and aqueous (50 wt %) glycerol systems, respectively. In the absence of an infrared objective,[41] the 1550 nm laser is focused normally through the Linkam front window (working distance <5 mm) by a separate aspheric lens with f = 7.5 mm (Thorlabs A375TM-C). In order to find the probe focus, the heating laser is scanned over the sample surface and the spectrum observed in real-time until the optimal position is reached. The chopper frequency is then set between 100 and 500 Hz with a view to maximizing the transient temperature rise contribution to the cycle, and the acquisition is run for some 3−6 h. Checks for any stability issues (alignment, cryostat failure, etc.) are conducted both during the experiment and on the final data file.

RESULTS AND DISCUSSION

Comparison data from quasi-static BLS is only available for the higher viscosity system i.e. pure glycerol, which is hence the starting point for demonstrating FBS feasibility. The time-evolution of the Brillouin frequency-shift of glycerol (Figure 2a, with heating at 100 Hz chopper frequency and 25% duty cycle) is the basic quantity in FBS for deducing the temperature-dependent phonon frequency (and, hence, T_g). Considering film dimensions (∼2 μm) Brillouin scattering occurs from phonon modes of the bulk material, here associated with the longitudinal sound velocity; for thinner supported films, multiple reflections from surface and interface can form standing acoustic waves and the BLS spectrum consists of several interference controlled peaks.[42] Similar to conventional BLS at fixed temperature, the reported frequency values are then obtained from a Lorentzian representation of the glycerol phonon peak in the experimental spectra at fixed time. As mentioned, pure glycerol does not absorb at the heating wavelength of 1550 nm, so a spin-cast polystyrene (PS) film (Figure 1) containing infrared dye is heated in its stead. Accordingly, it is necessary to distinguish the glycerol from the PS signal, and a double Lorentzian fit to the longitudinal phonon peaks of PS (lower) and glycerol (higher frequency) has to be performed. This is illustrated in the inset of Figure 2a, where spectra are recorded on the heating cycle, that is, the portion before the 4 ms mark. The glycerol phonon peak is seen to broaden and approach, but not cross, the more weakly temperature-dependent peak of the glassy PS.

In order to extract T_g from this plot, the time variable has to be eliminated and replaced with temperature, yielding the temperature-dependent phonon frequency $f(T)$. Hence, knowledge of not only the time-dependent Brillouin frequency-shift $f(t)$, but also temperature time-evolution $T(t)$ is necessary. There are several approaches to obtaining this information: Since the initial temperature $T_i = T(t_0)$ = 123 K is known and the behavior of $f(t)$ at temperature above T_g in the equilibrium liquid is not expected to depend on scan rate, it might be tempting to fit a curve between T_i and the deduced maximum temperature values. Unfortunately, there does not seem to be an easy analytical formula for $T(t)$. Indeed, some models[43] predict an indefinite temperature rise with square-root of time, and simulations of laser heating of water films have been shown to disagree[44] with experiment for higher powers. Experimentally, a number of time-resolved optical thermometry methods exist,[45] with fluorescent ones[44] being particularly popular and Raman-based ones[46,47] holding maybe the most long-term promise here. However, Brillouin spectrometry also offers options for temperature measurement,[48] based mainly on monitoring frequency-shift $f(t)$ and intensity $I(t)$.

In order to determine $T(t)$, we first use the Brillouin frequency-shift for temperature sensing, where the PS film provides a convenient additional phonon frequency f_{PS} for reference. Indeed, for heating not exceeding T_g, amorphous polymers show a weak but linear temperature-dependence of the frequency, independent of scan rate; above T_g, sensitivity increases, but photomechanical ablation[49] can become an issue. Accordingly, we plot $f_{PS}(t)$ from the double-Lorentzian representation of the BLS spectra (inset of Figure 2a) to obtain a first temperature reference, which produces a time-evolution curve as in Figure 2b (green symbols). However, while $f(t)$ of glycerol is monotonically decreasing, $f_{PS}(t)$ saturates in spite of rising temperature. The former, alongside increasing $I_{PS}(t)$ in Figure 2b (red broken line), indicates that PS temperature does rise concomitantly, so an explanation might be change of $f_{PS}(t)$ at high scan rate. In order to estimate $T(t)$ from $f_{PS}(t)$, it is also necessary to know the PS frequency-shift temperature differential α, where $f_{PS}(T) = f_0(1 - \alpha T)$. In principle, the slope α is a material property but in practice values ranging from 3×10^{-4} K^{-1} to 8×10^{-4} K^{-1} have been reported[50,51] for the glassy state (<373 K). Hence, we only exploit the linearity of f_{PS} in temperature and adjust the slope until glycerol frequencies at high temperature from FBS overlap with those from quasi-static BLS, while the known T_i controls the offset. The result can be seen in Figure 2c, where quasi-static BLS data points (upright pink crosses) reported in the temperature scale provided by the top x-axis with $\alpha = 3.6 \times 10^{-4}$ K^{-1} (see next paragraph for bottom x-axis) achieve coincidence on the heating cycle at least (f_0 = 15.8 GHz). Horizontal error bars

https://dx.doi.org/10.1021/acsphotonics.0c01533
ACS Photonics 2021, 8, 531−539

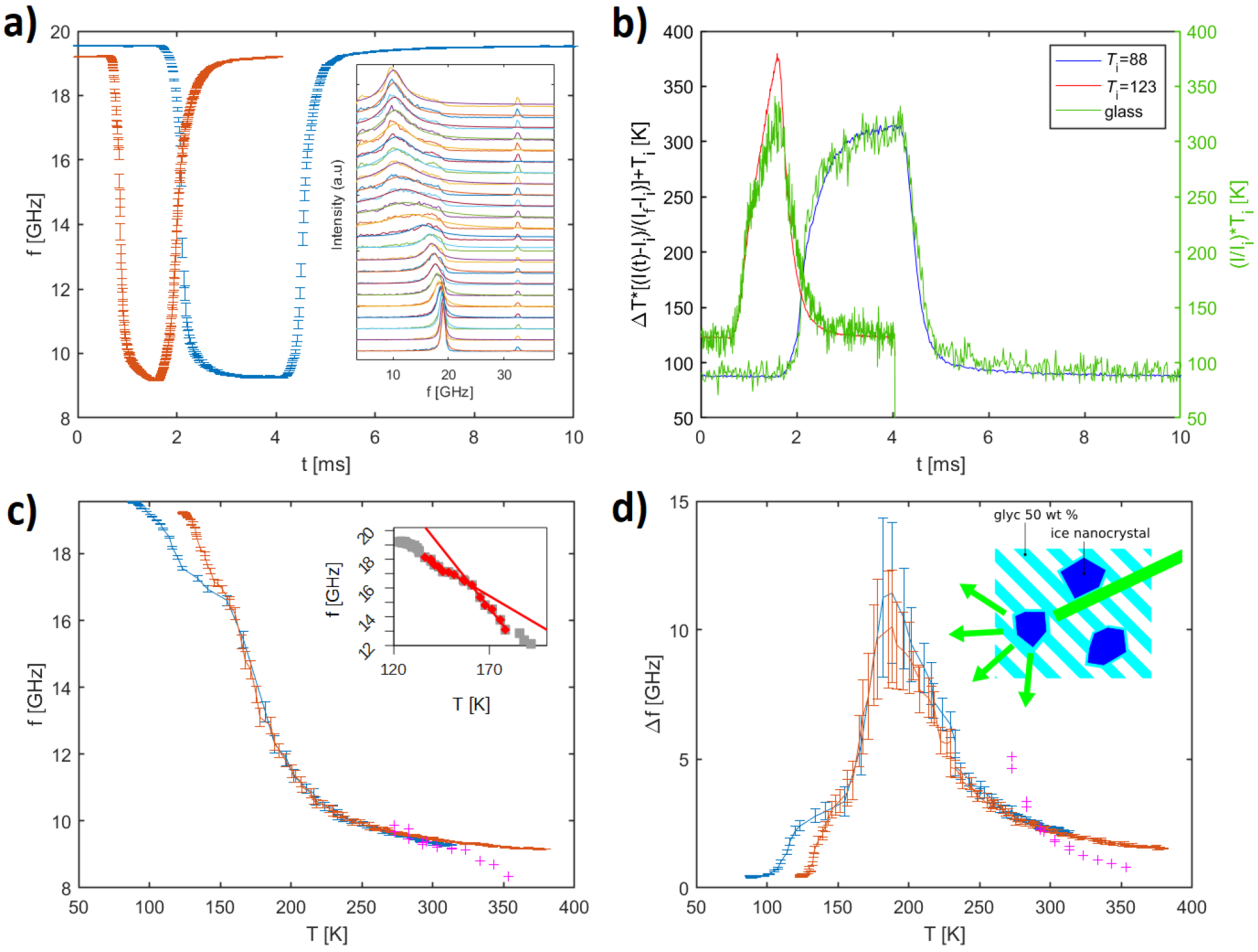

Figure 3. Representative FBS data for aqueous (50 wt %) glycerol: (a) time-evolution of the phonon frequency $f(t)$, for both T_i = 88 (blue, 100 Hz) and 123 K (red, 250 Hz), obtained from the Lorentzian representation of the BLS spectra; inset: selected spectra (T_i = 88 K), sampled on the heating cycle (Δt = 0.02 ms); (b) time-evolution of temperatures deduced from integrated detector counts $I(t)$, for both the glass substrate according to $(I/I_i) \times T_i$ (in green) and the glycerol/water mixture according to the formula on the left-hand y-axis (in blue and red), with $\Delta T(T_i)$ for the latter matched to glass substrate temperatures; (c) frequency-shift $f(T)$ of glycerol/water mixture against temperature, calibrated using temperatures from (b), for T_i = 88 K (blue) and T_i = 123 K (red); reasonable agreement with quasi-static BLS points (crosses) above the melting point, but somewhat low T_g = 161 K (upper right inset, showing T_i = 123 K case) are found; (d) similar to (c), but showing line width Δf on the y-axis, with the inset illustrating how direction of incident light (thick green line) is randomized (and, hence, line width broadened) through scattering by ice nanocrystals.

are large, but the T_g "kink" is clearly in evidence and leads to a value of T_g = 191 K (inset to Figure 2c). While in good agreement with T_g = 187 K from quasi-static BLS,[17] the T_g upshift at high scan rate seems too low considering the large frequency difference between the quenched and nonquenched glasses measured by FBS and quasi-static BLS respectively. The lower sound velocity for the former is due to less dense packing (larger fraction of free volume),[52] a circumstance confirmed by previous[22] BLS studies of time-dependent material response to a shallow (2−5 K) temperature step. Time-evolution in these cases, however, occurred over several hours, while entirely different time-scales are accessed by FBS.

Other than frequency-shift, tracking intensity of light scattered by an acoustic phonon can be a means of temperature calibration.[48] Due to linearity in k_BT, intensity can be expected to show much higher temperature sensitivity than the ∼10% increase observed in Figure 2b for f_{PS}. Moreover, while for the latter only $f_i = f(T_i)$ is known due to large uncertainty on α, for intensity we can conveniently assume $I(T = 0\ \mathrm{K}) = 0$, in addition to $I_i = I(t_0) = I(T_i)$; hence, $T \approx I(t) \times (T_i/I_i)$, meaning that not only relative but also absolute temperature information is gained. On the other hand, intensity also depends on density ρ and isothermal compressibility, both of which are potentially functions of temperature. For the PS film at least (as, e.g., for silica glass[48]), high linearity can be assumed, and it is accordingly interesting to compare peak area from the Lorentzian representation (red broken line in Figure 2b), which corresponds to intensity $I_{PS}(t)$, with frequency-shift evolution. On the heating cycle, there is good agreement for lower temperatures, whereas a rapid drop-off not mirrored by the frequency-shift is in evidence for the quench. The reason may be the more homogeneous temperature distribution during heating, since the laser heats dye distributed throughout the depth of the polystyrene, and heat does not have to diffuse first through the film. Using typical thermal diffusivity values of $D \sim 10^{-7}$ m^2/s,[53] we would however not expect the relevant diffusion time scales following formula $w^2/4D$ to much exceed the chosen histogram time-bin width (∼10 μs), for film thickness w = 2 μm at least. Finally, identifying frequency shift with I/I_i (right-hand axis of Figure 2b) translated to temperature as above, another estimate for $\alpha = 4.4 \times 10^{-4}$ K^{-1} (f_0 = 16.0 GHz) can

https://dx.doi.org/10.1021/acsphotonics.0c01533
ACS Photonics 2021, 8, 531−539

be obtained, corresponding to the bottom x-axis in Figure 2c. This value, however, seems to underestimate the glycerol temperature rise, since quasi-static BLS data points (tilted crosses in Figure 2c) lie too far right of the FBS curve, and the corresponding T_g = 178 K is somewhat low.

While temperature-calibration based on PS intensity has got a solid methodological foundation, the signal is rather noisy, presumably due to difficulties with the Lorentzian fit upon growing proximity of PS and glycerol phonons (Figure 2a). Hence, it is interesting to see if summing detector counts at each time instant can replace the need for the Lorentzian. For the sake of simplicity, we do not distinguish intensities of glycerol and PS, but integrate over both, heuristically neglecting any potentially nonlinear behavior of the former in temperature. The result is shown as a solid blue line in Figure 2b: On the heating flank, detector counts $I(t)$ match the PS reference intensity $I_{PS}(t)$ surprisingly well, though again there are deviations on the cooling cycle. In contrast to what we saw for $f_{PS}(t)$ (Figure 2c), this good correspondence concerns not only shape, but also dimensionless I/I_i values reported on the right-hand axis of Figure 2c. Trivially, a temperature estimate is then obtained from $(I/I_i) \times T_i$ and leads to the bottom x-axis calibration in Figure 2d. Alternatively, and as before, we can also impose agreement with quasi-static BLS data (crosses) of glycerol for higher temperatures, which leads to the top x-axis calibration (tilted crosses refer to bottom x-axis, upright crosses to top x-axis). For the latter, there is clearly a zone of good agreement close to T_g, though further out, the detector count calibration method seems to overestimate temperatures (again, only the heating cycle is considered). A reason might be overall change in sample optical properties that affect scattered light transmission. From the zone of good agreement, our T_g estimate is T_g = 200 K, which is higher than the literature value (T_g = 187 K as above) for quasi-static BLS, but compatible with the expected influence of quench rate due the low fragility[54] of glycerol (T_g = 185 K from the bottom x-axis in Figure 2d).

The pure glycerol case is useful for demonstrating FBS feasibility and to establish the procedure of temperature calibration. More interesting, however, is the case of the aqueous glycerol solution (50 wt %, equivalently 15 mol % or 5.5 M), which cannot be measured at low temperature by conventional BLS. This is a widely studied[55,56] but not trivial system. Indeed, a particular difficulty often arises from spatial heterogeneity in glycerol distribution,[31] control of which was outside the scope of the present experiment. The procedure is similar to that for the pure glycerol, with two adaptations: First, to obviate need for the double Lorenztian, the PS film is removed, since the 1550 nm laser can now heat the system under study directly. In order to have a reference against which to check that aqueous glycerol solution intensity still gives a good calibration variable, the FSR is widened to 40 GHz. This allows for the glass substrate longitudinal phonon to be observed, which replaces PS as intensity-based reference thermometer. Second, due to spatial heterogeneity, high temperature results from quasi-static BLS (which, involving the liquid state, present a spatial average) can no longer be expected to necessarily correspond with those from FBS. However, as we have seen (crosses in Figure 2d), absolute temperatures from $(I/I_i) \times T_i$ are not always reliable, so a means of counterchecking is desirable. To this end, the same measurement is run twice in a row, with two different initial temperatures T_i = 88 and 123 K set on the cryostat. With offsets fixed by the two known T_i, we can then expect the two curves to coincide at high temperatures, for correctly calibrated slopes.

Figure 3a shows the time-evolution of the Brillouin frequency-shift $f(t)$ for the glycerol/water (50 wt %) mixture, considering both initial temperatures. Chopper frequency (Figure 3a,b) was slightly increased for the FBS run at T_i = 123 K, in order to allow for higher resolution sampling. Representative spectra (heating cycle for T_i = 88 K) are shown in the inset and represented by a single Lorentzian line (in view of broad spectra at intermediate times, to be discussed further below, a double Lorentzian fit was also attempted but not found to more consistently capture the shape deformation, which might additionally be influenced by Mie scattering); the glass substrate phonon at frequencies higher than 30 GHz was excluded from the fit. Time-evolution of integrated counts from aqueous glycerol $I(t)$, intended for use as the time-resolved temperature probe, is shown (blue and red lines) in Figure 3b, and compared with results from the reference peak (green lines). The latter is now provided by the glass substrate integrated counts (peak above 30 GHz) rather than the PS fit, but its density ρ and compressibility can be expected to be at least as constant with temperature as for the glassy polymer. Shape-wise and for T_i = 88 K, there is good agreement; for T_i = 123 K, glass substrate final temperature T_f seems too close to T_f of the T_i = 88 K case considering 35 K difference in their T_i, but temperatures from aqueous glycerol overestimate T_f, far from T_g. In contrast to what we did for Figure 2b, however, this comparison only concerns normalized values I/I_i for the glass substrate, to which the two temperature rise values $\Delta T = T_f - T_i$ for the aqueous glycerol curves are then matched. Though $\Delta T(T_i = 88\ K) = 227$ K, but $\Delta T(T_i = 123\ K) \sim 260$ K, which might be, for example, due to temperature-dependent absorption at 1550 nm or transmission at 532 nm, low-temperature behavior is reasonably robust to uncertainties on T_f. Thus, convincing agreement in the vicinity of T_g is obtained in spite of the large uncertainties of density ρ and sound velocity further out. Considering only the heating cycle, elimination of the time-variable thus leads to traces of phonon frequency against temperature $f(T)$ for the two T_i, as in Figure 3c. As stated above, spatial microheterogeneity renders any comparison with quasi-static BLS dubitable even where data points for the latter (crosses in Figure 3c) pertain to temperatures above the melting point of ice. Nevertheless, confirmation of the technique can be obtained by comparing the curves from two different T_i. At high temperature, the two ΔT chosen above produce convincing correspondence, while at low temperatures, behavior is clearly different regarding slope, even though they intersect near the same T_g (inset to Figure 3c). Along with the bumpiness of the $f(T)$ curve for T_i = 88 K in the sub-T_g region, this might hint at the existence of a kinetic process allowing for structural changes even in the glassy state, as reported[57] for phase change materials, likewise a class of systems with high crystallization rates. Another hypothesis might be that heating to lower T_f for T_i = 88 K allows a greater fraction of ice to remain, resulting in lower plasticization by water.

More numerically, from Figure 3c, below T_g, we find slopes $\alpha = 2.1 \times 10^{-3}\ K^{-1}$ and $2.7 \times 10^{-3}\ K^{-1}$ for T_i = 88 and 123 K, respectively; above T_g, the slope is $3.9 \times 10^{-3}\ K^{-1}$ for both. While this seems huge compared to glassy pure glycerol ($\alpha = 2.8 \times 10^{-4}\ K^{-1}$ in Figure 2d) or, for example, PS slopes as

https://dx.doi.org/10.1021/acsphotonics.0c01533
ACS Photonics 2021, 8, 531−539

above, from ultrasonic data[58] we graphically estimate a slope of $\sim 2 \times 10^{-3}$ K^{-1} for 68 mol %, above T_g (though ultrasonic behavior can be expected[59] to slightly deviate from hypersonic). This large disparity expressed in the values of α reflects the different H-bonded structures of the two systems. Alternatively, it might relate to plasticization effects also observed in diblock copolymers.[60] A greater cause of concern is the T_g value obtained: The "kink" (inset to Figure 3c) is around 161 K, but literature indicates a value of 170 K,[61,56,62] which should be independent of concentration for less than 60 wt % solutions. One possible origin might be to suppose that part of the water was able to crystallize out, leaving behind a higher concentration glycerol solution (e.g., the MFCS). Indeed, the quench rate of 30 K/min permitted by our cryostat is slightly below the reported[63] critical cooling rate for 50 wt % solution. This explanation could account for values $T_g \sim 160$ K. Alternatively, the reason could simply be poor fit quality (larger error bars above T_g in Figure 3c) of the single Lorentzian model for some of the spectra (inset of Figure 3a), probably due to residual ice, which causes ill-defined laser incidence direction (inset of Figure 3d), as well as additional acoustic losses. Ice formation is somewhat surprising for 50 wt % glycerol because critical heating rate at this concentration is said to be around 10^3 K/s,[63] while our rates exceed 10^5 K/s. However, its presence is confirmed by a small high frequency shoulder around ∼20 GHz, which remains immobile and emerges from the much stronger main peak at high temperatures (in the intermediate region, it is not clearly resolved, whence preference of the single over the double Lorentzian fit). This frequency range is consistent with reported[64] low-temperature sound velocities of ∼4000 m/s for hexagonal ice crystals with sizes exceeding the effective medium phonon wavelength (∼180 nm). In this case, FBS operates as an elastic impedance contrast based imaging technique with submicrometer spatial resolution.[65] In part, however, this hypothesis on ice-crystal formation is also corroborated by the proximity to T_g of the hypersonic loss maximum (Figure 3d) seen at 200 K. The latter should not be confused with the typical structural relaxation driven loss peak, which would be expected around 250 K based on dielectric data.[66,56] Other than scattering laser light (inset of Figure 3d), ice crystals increase hypersonic attenuation in analogy to what has been reported[67] for concentrated colloid dispersions. This circumstance can possibly have a detrimental knock-on effect on axial spatial resolution at least, coupled to phonon lifetime as we just mentioned.[68] Above T_g but below the freezing point of water, the initially huge line width decreases again, maybe because of nanocrystal disappearance enabled by their depressed melting point at small size.[69] Otherwise, the nanocrystals might belong to a metastable ice precursor phase reported[70,71] for this temperature range. The resemblance of the step-like Δf shape (Figure 3d) to the $f(T)$ curve between 100 and 125 K corroborates the notion of the presence of sufficient ice nanocrystals that can increase the hypersonic attenuation. The second increase of Δf above 150 K marks the glass transition temperature, sensed here via a change of the dynamic viscosity η at T_g following $\Delta f \sim \eta/\rho$.

CONCLUSION

We have demonstrated "Flash Brillouin Scattering" (FBS), a new method for measuring the glass transition temperature at high scan rates, based on time-resolved Brillouin confocal microscopy and capable of high spatial resolution in situ probing. Proof-of-principle was accomplished by comparing results on pure glycerol with data from quasi-static Brillouin scattering. Temperature calibration was recognized to be the main challenge, but an easy if possibly not universally applicable method, based on integrating detector counts and exploiting the glass substrate as reference, was found to give credible results. Turning toward its aqueous mixture (50 wt %), feasibility of FBS could thus be proven notwithstanding various system-specific issues, to be attributed probably to its spatial heterogeneity and imprecise control. However, in the practical context where glycerol/water is often studied, namely, cryopreservation of biological material by vitrification, our Brillouin-spectroscopy based "flash T_g" method would likely be integrated into a Raman confocal microscope,[31] as already in use in the discipline. In this configuration, Raman data would allow for precise concentration knowledge and offer various additional thermometry options. On the Brillouin front as well, however, we hope that the present study will spur improvements in temperature-sensing capabilities, for example, by identifying materials with high frequency-shift differentials. Also, the main drawback of the current experiment with a Fabry−Perot interferometer (FPI) are very long acquisition times, incompatible with any potential imaging applications. Though in part to blame on FPI-parameters such as detector choice,[29] a factor of at least 50 could be gained[72] if a prism-type ("Virtually Imaged Phased Array") spectrometer could be employed.[26] By minimizing laser flash exposure duration, the latter strategy would also allow for exploring systems where high scan rates can lead to photomechanical ablation, not an issue in the present study, but a concern with, e.g., polymer thin films.[49] Considering its out-of-the-box high temporal resolution and otherwise excellent performance, FPI-based FBS is however likely to remain the reference solution for the foreseeable future.

AUTHOR INFORMATION

Corresponding Author

Konrad Rolle − *Max-Planck-Institute for Polymer Research, 55128 Mainz, Germany;* orcid.org/0000-0002-7291-3285; Email: rolle@mpip-mainz.mpg.de

Authors

Hans-Jürgen Butt − *Max-Planck-Institute for Polymer Research, 55128 Mainz, Germany;* orcid.org/0000-0001-5391-2618

George Fytas − *Max-Planck-Institute for Polymer Research, 55128 Mainz, Germany;* orcid.org/0000-0003-2504-6374

Complete contact information is available at: https://pubs.acs.org/10.1021/acsphotonics.0c01533

Funding

K.R. and G.F. acknowledge financial support by ERC AdG SmartPhon (Grant No. 694977).

Notes

The authors declare no competing financial interest.

ACKNOWLEDGMENTS

We thank Werner Steffen for helpful discussions on photon correlation spectroscopy. We thank Xiaomin Liu for assistance with the fiber optics.

REFERENCES

(1) Schick, C.; Mathot, V. *Fast Scanning Calorimetry*; Springer, 2016.
(2) Beaucage, G.; Composto, R.; Stein, R. S. Ellipsometric Study of the Glass-Transition and Thermal-Expansion Coefficients of Thin Polymer-Films. *J. Polym. Sci., Part B: Polym. Phys.* **1993**, *31* (3), 319−326.
(3) Keddie, J. L.; Jones, R. A. L.; Cory, R. A. Size-Dependent Depression of the Glass-Transition Temperature in Polymer-Films. *Europhys. Lett.* **1994**, *27* (1), 59−64.
(4) Forrest, J. A.; DalnokiVeress, K.; Stevens, J. R.; Dutcher, J. R. Effect of free surfaces on the glass transition temperature of thin polymer films. *Phys. Rev. Lett.* **1996**, *77* (10), 2002−2005.
(5) Scarcelli, G.; Yun, S. H. Confocal Brillouin microscopy for three-dimensional mechanical imaging. *Nat. Photonics* **2008**, *2* (1), 39−43.
(6) Kennedy, B. F.; Wijesinghe, P.; Sampson, D. D. The emergence of optical elastography in biomedicine. *Nat. Photonics* **2017**, *11* (4), 215−221.
(7) Hammiche, A.; Reading, M.; Pollock, H. M.; Song, M.; Hourston, D. J. Localized thermal analysis using a miniaturized resistive probe. *Rev. Sci. Instrum.* **1996**, *67* (12), 4268−4274.
(8) Pollock, H. M.; Hammiche, A. Micro-thermal analysis: techniques and applications. *J. Phys. D: Appl. Phys.* **2001**, *34* (9), R23−R53.
(9) Nelson, B. A.; King, W. P. Measuring material softening with nanoscale spatial resolution using heated silicon probes. *Rev. Sci. Instrum.* **2007**, *78* (2), 023702.
(10) Nikiforov, M. P.; Gam, S.; Jesse, S.; Composto, R. J.; Kalinin, S. V. Morphology Mapping of Phase-Separated Polymer Films Using Nanothermal Analysis. *Macromolecules* **2010**, *43* (16), 6724−6730.
(11) Guen, E.; Klapetek, P.; Puttock, R.; Hay, B.; Allard, A.; Maxwell, T.; Chapuis, P.-O.; Renahy, D.; Davee, G.; Valtr, M.; Martinek, J.; Kazakova, O.; Gomes, S. SThM-based local thermo-mechanical analysis: Measurement intercomparison and uncertainty analysis. *Int. J. Therm. Sci.* **2020**, *156*, 106502.
(12) Giridharagopal, R.; Rayermann, G. E.; Shao, G. Z.; Moore, D. T.; Reid, O. G.; Tillack, A. F.; Masiello, D. J.; Ginger, D. S. Submicrosecond Time Resolution Atomic Force Microscopy for Probing Nanoscale Dynamics. *Nano Lett.* **2012**, *12* (2), 893−898.
(13) Costa, L.; Li-Destri, G.; Pontoni, D.; Konovalov, O.; Thomson, N. H. Liquid-Liquid Interfacial Imaging Using Atomic Force Microscopy. *Adv. Mater. Interfaces* **2017**, *4* (16), 1700203.
(14) Natesan, H.; Bischof, J. C. Multiscale Thermal Property Measurements for Biomedical Applications. *ACS Biomater. Sci. Eng.* **2017**, *3* (11), 2669−2691.
(15) Karlsson, J. O. M.; Cravalho, E. G.; Toner, M. A Model of Diffusion-Limited Ice Growth inside Biological Cells during Freezing. *J. Appl. Phys.* **1994**, *75* (9), 4442−4445.
(16) Khosla, K.; Wang, Y. R.; Hagedorn, M.; Qin, Z. P.; Bischof, J. Gold Nanorod Induced Warming of Embryos from the Cryogenic State Enhances Viability. *ACS Nano* **2017**, *11* (8), 7869−7878.
(17) Comez, L.; Fioretto, D.; Scarponi, F.; Monaco, G. Density fluctuations in the intermediate glass-former glycerol: A Brillouin light scattering study. *J. Chem. Phys.* **2003**, *119* (12), 6032−6043.
(18) Inaba, A.; Andersson, O. Multiple glass transitions and two step crystallization for the binary system of water and glycerol*. *Thermochim. Acta* **2007**, *461* (1−2), 44−49.
(19) Kojima, S. Low-Frequency Raman Investigation of the Liquid-Glass Transition in Glycerol. *Phys. Rev. B: Condens. Matter Mater. Phys.* **1993**, *47* (5), 2924−2927.
(20) Liem, H.; Cabanillas-Gonzalez, J.; Etchegoin, P.; Bradley, D. D. C. Glass transition temperatures of polymer thin films monitored by Raman scattering. *J. Phys.: Condens. Matter* **2004**, *16* (6), 721−728.
(21) Menezes, D. B.; Reyer, A.; Marletta, A.; Musso, M. Glass transition of polystyrene (PS) studied by Raman spectroscopic investigation of its phenyl functional groups. *Mater. Res. Express* **2017**, *4* (1), 015303.
(22) Krüger, J.-K.; Alnot, P.; Baller, J.; Bactavatchalou, R.; Dorosz, S.; Henkel, M.; Kolle, M.; Krüger, S. P.; Müller, U.; Philipp, M., About the nature of the structural glass transition: An experimental approach. *Ageing and the Glass Transition*; Springer, 2007; pp 61−159.
(23) Cheng, W.; Sainidou, R.; Burgardt, P.; Stefanou, N.; Kiyanova, A.; Efremov, M.; Fytas, G.; Nealey, P. F. Elastic properties and glass transition of supported polymer thin films. *Macromolecules* **2007**, *40* (20), 7283−7290.
(24) Voudouris, P.; Gomopoulos, N.; Le Grand, A.; Hadjichristidis, N.; Floudas, G.; Ediger, M. D.; Fytas, G. Does Brillouin light scattering probe the primary glass transition process at temperatures well above glass transition? *J. Chem. Phys.* **2010**, *132* (7), 074906.
(25) Shirasaki, M. Large angular dispersion by a virtually imaged phased array and its application to a wavelength demultiplexer. *Opt. Lett.* **1996**, *21* (5), 366−368.
(26) Steelman, Z. A.; Weems, A. C.; Traverso, A. J.; Szafron, J. M.; Maitland, D. J.; Yakovlev, V. V. Revealing the glass transition in shape memory polymers using Brillouin spectroscopy. *Appl. Phys. Lett.* **2017**, *111* (24), 241904.
(27) Büttner, O.; Bauer, M.; Rueff, A.; Demokritov, S. O.; Hillebrands, B.; Slavin, A. N.; Kostylev, M. P.; Kalinikos, B. A. Space-and time-resolved Brillouin light scattering from nonlinear spin-wave packets. *Ultrasonics* **2000**, *38* (1−8), 443−449.
(28) Meng, Z.; Bustamante Lopez, S. C.; Meissner, K. E.; Yakovlev, V. V. Subcellular measurements of mechanical and chemical properties using dual Raman-Brillouin microspectroscopy. *J. Biophotonics* **2016**, *9* (3), 201−207.
(29) Scarponi, F.; Mattana, S.; Corezzi, S.; Caponi, S.; Comez, L.; Sassi, P.; Morresi, A.; Paolantoni, M.; Urbanelli, L.; Emiliani, C.; Roscini, L.; Corte, L.; Cardinali, G.; Palombo, F.; Sandercock, J. R.; Fioretto, D. High-Performance Versatile Setup for Simultaneous Brillouin-Raman Microspectroscopy. *Phys. Rev. X* **2017**, *7* (3), 031015.
(30) Stracke, F.; Kreiner-Moller, A.; Zimmermann, H. Laser Scanning Microscopy in Cryobiology. *Methods Mol. Biol.* **2015**, *1257*, 229−241.
(31) Dong, J. P.; Hubel, A.; Bischof, J. C.; Aksan, A. Freezing-Induced Phase Separation and Spatial Microheterogeneity in Protein Solutions. *J. Phys. Chem. B* **2009**, *113* (30), 10081−10087.
(32) Dong, J. P.; Malsam, J.; Bischof, J. C.; Hubel, A.; Aksan, A. Spatial Distribution of the State of Water in Frozen Mammalian Cells. *Biophys. J.* **2010**, *99* (8), 2453−2459.
(33) Okotrub, K. A.; Amstislavsky, S. Y.; Surovtsev, N. V. Raman spectroscopy reveals the lipid phase transition in preimplantation mouse embryos during freezing. *Arch. Biochem. Biophys.* **2017**, *635*, 37−43.
(34) Steif, P. S.; Palastro, M. C.; Rabin, Y. The effect of temperature gradients on stress development during cryopreservation via vitrification. *Cell Preserv. Technol.* **2007**, *5* (2), 104−115.
(35) Yap, B.; Shichijyo, S.; Matsushige, K.; Takemura, T. Brillouin-Scattering from Pmma under Uniaxial Tensile-Stress. *Jpn. J. Appl. Phys. 2* **1982**, *21* (8), L523−L525.
(36) Caponi, S.; Corezzi, S.; Mattarelli, M.; Fioretto, D. Stress effects on the elastic properties of amorphous polymeric materials. *J. Chem. Phys.* **2014**, *141* (21), 214901.
(37) Molteni, M.; Ferri, F. Commercial counterboard for 10 ns software correlator for photon and fluorescence correlation spectroscopy. *Rev. Sci. Instrum.* **2016**, *87* (11), 113108.
(38) Hall, D. B.; Underhill, P.; Torkelson, J. M. Spin coating of thin and ultrathin polymer films. *Polym. Eng. Sci.* **1998**, *38* (12), 2039−2045.
(39) Shapovalov, V.; Zaitsev, V. S.; Strzhemechny, Y.; Choudhery, F.; Zhao, W.; Schwarz, S. A.; Ge, S. R.; Shin, K.; Sokolov, J.; Rafailovich, M. H. Nanostructure formation in spin-cast polystyrene films. *Polym. Int.* **2000**, *49* (5), 432−436.
(40) Slayton, R. M.; Nelson, K. A. Picosecond acoustic transmission measurements. II. Probing high frequency structural relaxation in supercooled glycerol. *J. Chem. Phys.* **2004**, *120* (8), 3919−3930.
(41) Hajireza, P.; Shi, W.; Bell, K.; Paproski, R. J.; Zemp, R. J. Non-interferometric photoacoustic remote sensing microscopy. *Light: Sci. Appl.* **2017**, *6*, e16278.

https://dx.doi.org/10.1021/acsphotonics.0c01533
ACS Photonics 2021, 8, 531−539

(42) Gomopoulos, N.; Cheng, W.; Efremov, M.; Nealey, P. F.; Fytas, G. Out-of-Plane Longitudinal Elastic Modulus of Supported Polymer Thin Films. *Macromolecules* **2009**, *42* (18), 7164−7167.
(43) Yager, K. G.; Barrett, C. J. Temperature modeling of laser-irradiated azo-polymer thin films. *J. Chem. Phys.* **2004**, *120* (2), 1089−1096.
(44) Cordero, M. L.; Verneuil, E.; Gallaire, F.; Baroud, C. N. Time-resolved temperature rise in a thin liquid film due to laser absorption. *Phys. Rev. E* **2009**, *79* (1), 011201.
(45) Brites, C. D. S.; Lima, P. P.; Silva, N. J. O.; Millan, A.; Amaral, V. S.; Palacio, F.; Carlos, L. D. Thermometry at the nanoscale. *Nanoscale* **2012**, *4* (16), 4799−4829.
(46) Sinclair, M. B.; Haaland, D. M.; Timlin, J. A.; Jones, H. D. T. Hyperspectral confocal microscope. *Appl. Opt.* **2006**, *45* (24), 6283−6291.
(47) Kojima, J.; Fischer, D.; Nguyen, Q. V. Subframe burst gating for Raman spectroscopy in combustion. *Opt. Lett.* **2010**, *35* (9), 1323−1325.
(48) Birt, D. R.; An, K.; Weathers, A.; Shi, L.; Tsoi, M.; Li, X. Q. Brillouin light scattering spectra as local temperature sensors for thermal magnons and acoustic phonons. *Appl. Phys. Lett.* **2013**, *102* (8), 082401.
(49) Kappes, R. S.; Schonfeld, F.; Li, C.; Golriz, A. A.; Nagel, M.; Lippert, T.; Butt, H. J.; Gutmann, J. S. A study of photothermal laser ablation of various polymers on microsecond time scales. *SpringerPlus* **2014**, *3*, 489.
(50) Oh, S. H.; Lee, B. W.; Ko, J. H.; Lee, H.; Park, J.; Ko, Y. H.; Kim, K. J. Temperature and molecular-weight dependences of acoustic behaviors of polystyrene studied using Brillouin spectroscopy. *J. Korean Phys. Soc.* **2017**, *70* (8), 791−795.
(51) Cang, Y.; Reuss, A. N.; Lee, J.; Yan, J. J.; Zhang, J. N.; Alonso-Redondo, E.; Sainidou, R.; Rembert, P.; Matyjaszewski, K.; Bockstaller, M. R.; Fytas, G. Thermomechanical Properties and Glass Dynamics of Polymer-Tethered Colloidal Particles and Films. *Macromolecules* **2017**, *50* (21), 8658−8669.
(52) Kovacs, A. J. La Contraction Isotherme Du Volume Des Polymeres Amorphes. *J. Polym. Sci.* **1958**, *30* (121), 131−147.
(53) Rouabah, F.; Dadache, D.; Haddaoui, N. Thermophysical and mechanical properties of polystyrene: influence of free quenching. *ISRN Polym. Sci.* **2012**, *2012*, 1.
(54) Lunkenheimer, P.; Pimenov, A.; Schiener, B.; Bohmer, R.; Loidl, A. High-frequency dielectric spectroscopy on glycerol. *Europhys. Lett.* **1996**, *33* (8), 611−616.
(55) Li, D. X.; Liu, B. L.; Liu, Y. S.; Chen, C. L. Predict the glass transition temperature of glycerol-water binary cryoprotectant by molecular dynamic simulation. *Cryobiology* **2008**, *56* (2), 114−119.
(56) Popov, I.; Greenbaum, A.; Sokolov, A. P.; Feldman, Y. The puzzling first-order phase transition in water-glycerol mixtures. *Phys. Chem. Chem. Phys.* **2015**, *17* (27), 18063−18071.
(57) Pries, J.; Wei, S.; Wuttig, M.; Lucas, P. Switching between Crystallization from the Glassy and the Undercooled Liquid Phase in Phase Change Material Ge2Sb2Te5. *Adv. Mater.* **2019**, *31* (39), 1900784.
(58) Slie, W. M.; Donfor, A. R.; Litovitz, T. A. Ultrasonic Shear and Longitudinal Measurements in Aqueous Glycerol. *J. Chem. Phys.* **1966**, *44* (10), 3712−3718.
(59) Klieber, C.; Hecksher, T.; Pezeril, T.; Torchinsky, D. H.; Dyre, J. C.; Nelson, K. A. Mechanical spectra of glass-forming liquids. II. Gigahertz-frequency longitudinal and shear acoustic dynamics in glycerol and DC704 studied by time-domain Brillouin scattering. *J. Chem. Phys.* **2013**, *138* (12), 12A544.
(60) Aluculesei, A.; Pipertzis, A.; Piunova, V. A.; Miyake, G. M.; Floudas, G.; Fytas, G.; Grubbs, R. H. Thermomechanical Behavior and Local Dynamics of Dendronized Block Copolymers and Constituent Homopolymers. *Macromolecules* **2015**, *48* (12), 4142−4150.
(61) Zhao, L. S.; Cao, Z. X.; Wang, Q. Glass transition of aqueous solutions involving annealing-induced ice recrystallization resolves liquid-liquid transition puzzle of water. *Sci. Rep.* **2015**, *5*, 15714.
(62) Bachler, J.; Fuentes-Landete, V.; Jahn, D. A.; Wong, J.; Giovambattista, N.; Loerting, T. Glass polymorphism in glycerol-water mixtures: II. Experimental studies. *Phys. Chem. Chem. Phys.* **2016**, *18* (16), 11058−11068.
(63) Hopkins, J. B.; Badeau, R.; Warkentin, M.; Thorne, R. E. Effect of common cryoprotectants on critical warming rates and ice formation in aqueous solutions. *Cryobiology* **2012**, *65* (3), 169−178.
(64) Proctor, T. M. Low-Temperature Speed of Sound in Single-Crystal Ice. *J. Acoust. Soc. Am.* **1966**, *39*, 972.
(65) Priadilova, O.; Cheng, W.; Tommaseo, G.; Steffen, W.; Gutmann, J. S.; Fytas, G. Probing the micromechanical behavior of semicrystalline polypropylene films by Brillouin spectroscopy. *Macromolecules* **2005**, *38* (6), 2321−2326.
(66) Hayashi, Y.; Puzenko, A.; Balin, I.; Ryabov, Y. E.; Feldman, Y. Relaxation dynamics in glycerol-water mixtures. 2. Mesoscopic feature in water rich mixtures. *J. Phys. Chem. B* **2005**, *109* (18), 9174−9177.
(67) Riese, D. O.; Wegdam, G. H. Sound propagation in suspensions of colloidal spheres with viscous coupling. *Phys. Rev. Lett.* **1999**, *82* (8), 1676−1679.
(68) Mattarelli, M.; Vassalli, M.; Caponi, S. Relevant Length Scales in Brillouin Imaging of Biomaterials: The Interplay between Phonons Propagation and Light Focalization. *ACS Photonics* **2020**, *7* (9), 2319−2328.
(69) Pan, D.; Liu, L. M.; Slater, B.; Michaelides, A.; Wang, E. Melting the Ice: On the Relation between Melting Temperature and Size for Nanoscale Ice Crystals. *ACS Nano* **2011**, *5* (6), 4562−4569.
(70) Russo, J.; Romano, F.; Tanaka, H. New metastable form of ice and its role in the homogeneous crystallization of water. *Nat. Mater.* **2014**, *13* (7), 733−739.
(71) Buttersack, T.; Weiss, V. C.; Bauerecker, S. Hypercooling Temperature of Water is about 100 K Higher than Calculated before. *J. Phys. Chem. Lett.* **2018**, *9* (3), 471−475.
(72) Yan, G.; Bazir, A.; Margueritat, J.; Dehoux, T. Evaluation of commercial Virtually Imaged Phase Array and Fabry-Pérot based Brillouin spectrometers for applications to biology. *Biomed. Opt. Express* **2020**, *11*, 6933.

https://dx.doi.org/10.1021/acsphotonics.0c01533
ACS Photonics 2021, 8, 531−539